

RESEARCH ARTICLE

10.1002/2015JA022095

Density variations in the Earth's magnetospheric cusps

B. M. Walsh¹, J. Niehof², M. R. Collier³, D. T. Welling⁴, D. G. Sibeck⁵, F. S. Mozer⁶, T. A. Fritz¹, and K. D. Kuntz⁷

Key Points:

- Cusp electron density scales closely with the solar wind density
- Ionospheric contributions to the density in the cusp become dominant near four Earth radii
- Cusp high charge state oxygen density scales with solar wind density

Correspondence to:

B. M. Walsh,
bwalsh@bu.edu

Citation:

Walsh, B. M., J. Niehof, M. R. Collier, D. T. Welling, D. G. Sibeck, F. S. Mozer, T. A. Fritz, and K. D. Kuntz (2016), Density variations in the Earth's magnetospheric cusps, *J. Geophys. Res. Space Physics*, 121, 2131–2142, doi:10.1002/2015JA022095.

Received 31 OCT 2015

Accepted 18 FEB 2016

Accepted article online 19 FEB 2016

Published online 15 MAR 2016

¹Mechanical Engineering Department and Center for Space Physics, Boston University, Boston, Massachusetts, USA, ²Institute for the Study of Earth, Oceans, and Space, University of New Hampshire, Durham, New Hampshire, USA, ³Planetary Division, NASA Goddard Space Flight Center, Greenbelt, Maryland, USA, ⁴AOSS, University of Michigan, Ann Arbor, Michigan, USA, ⁵Heliophysics Division, NASA Goddard Space Flight Center, Greenbelt, Maryland, USA, ⁶Space Sciences Laboratory, University of California, Berkeley, California, USA, ⁷Henry A. Rowland Department of Physics and Astronomy, The Johns Hopkins University, Baltimore, Maryland, USA

Abstract Seven years of measurements from the Polar spacecraft are surveyed to monitor the variations of plasma density within the magnetospheric cusps. The spacecraft's orbital precession from 1998 through 2005 allows for coverage of both the northern and southern cusps from low altitude out to the magnetopause. In the mid- and high- altitude cusps, plasma density scales well with the solar wind density ($n_{\text{cusp}}/n_{\text{sw}} \sim 0.8$). This trend is fairly steady for radial distances greater than $4 R_E$. At low altitudes ($r < 4 R_E$) the density increases with decreasing altitude and even exceeds the solar wind density due to contributions from the ionosphere. The density of high charge state oxygen ($O^{>+2}$) also displays a positive trend with solar wind density within the cusp. A multifluid simulation with the Block-Adaptive-Tree Solar Wind Roe-Type Upwind Scheme MHD model was run to monitor the relative contributions of the ionosphere and solar wind plasma within the cusp. The simulation provides similar results to the statistical measurements from Polar and confirms the presence of ionospheric plasma at low altitudes.

1. Introduction

A necessary feature of a planetary dipole magnetic field is a cusp in each hemisphere with converging magnetic field lines. Early spacecraft measurements identified the cusps as the regions with the most direct entry of solar wind plasma into the Earth's magnetosphere [Heikkila and Winningham, 1971; Frank, 1971]. Over time, a number of in situ spacecraft have observed solar wind plasma in the cusp over a large range of radial distances from the low-altitude ionosphere [e.g., Newell and Meng, 1988; Woch and Lundin, 1992] out to the magnetopause [e.g., Haerendel et al., 1978; Farrell and Van Allen, 1990]. Statistical studies from the Viking [Aparicio et al., 1991] and Cluster spacecraft [Lavraud et al., 2004] show the density of plasma within the cusp to be greater than that in adjacent magnetospheric regions and to scale with the solar wind density.

We understand the terrestrial cusps and solar wind entry in terms of magnetic reconnection. The magnetic field lines threading the cusps extend outward and form the magnetopause. As reconnection occurs along the magnetopause, closed geomagnetic field lines become interconnected with those in the magnetosheath, and shocked solar wind plasma can flow freely along the newly opened field lines into the cusps. Observationally, the entry of solar wind plasma into the cusps is measured through a number of signatures. The composition within the cusps includes ion species of solar wind origin such as He^{++} [Shelley et al., 1976] as well as heavy solar wind ions [Kremser et al., 1995; Perry et al., 2000]. Particles also show a number of time-of-flight effects as consequences of newly opened magnetic field lines convecting tailward through the cusp. These time-of-flight effects include a temperature anisotropy T_{\perp}/T_{\parallel} increasing with latitude and time energy dispersions [Rosenbauer et al., 1975; Reiff et al., 1977]. Both the composition and time-of-flight effects indicate solar wind plasma being injected onto magnetospheric field lines opened through magnetopause reconnection.

Although the cusp density is greater than the adjacent magnetospheric regions, it is often structured due to these time-of-flight effects. During periods of steady magnetopause reconnection at the subsolar magnetopause, a peak in density is observed at the low-latitude edge of the cusp, while the density decreases with increasing latitude [Escoubet et al., 2008; Pitout et al., 2009]. For periods when steady reconnection occurs poleward of the cusp, a less defined density dispersion in the opposite direction, with the peak in density on

the poleward edge, is often observed. During periods of temporally variable reconnection or multiple reconnection lines, multiple density dispersions are observed, often overlapping. These structures within the cusps have been used as tracers for the location and variability of magnetopause reconnection [e.g., *Smith and Lockwood, 1990; Newell and Meng, 1991; Escoubet et al., 1992; Lockwood and Smith, 1994; Lockwood, 1995; Trattner et al., 1998*]. Although the shape of the density structures provides valuable information, the magnitude of density within the cusp as a function of radial distance also provides information about the efficiency of solar wind entry and is the focus of the current study.

Solar wind plasma within the terrestrial cusps is also important because it can undergo charge exchange with exospheric neutrals. In the process of solar wind charge exchange (sometimes referred to as SWCX in the literature), a high charge state ion collides with a neutral atom or molecule. Often, the high charge state ion from the solar wind is carbon or oxygen, while the most abundant neutral target species is often hydrogen. Through this interaction an electron is transferred from the neutral to the high charge state ion in an excited state. As the electron transitions to a lower energy state a soft X-ray photon is released. This can occur anywhere a plasma with high charge state ions interacts with neutral atoms such as comets [*Cravens, 1997*], planetary, and lunar environments [*Dennerl et al., 2002; Dennerl, 2002; Wargelin et al., 2004; Collier et al., 2014*], as well as the Earth [*Cravens et al., 2001; Snowden et al., 2004; Carter et al., 2011*]. Within the cusps, high charge state solar wind plasma can penetrate deep into the magnetosphere, and to smaller radial distances, where the neutral density is high. In these regions the ingredients for charge exchange are abundant and both modeling [*Robertson et al., 2006; Kuntz et al., 2015*] and observations [*Fujimoto et al., 2007*] have shown the soft X-ray emissions to be high. The current study quantifies the entry of solar wind plasma within the cusp as a function of solar wind density and radial distance within the cusp. This provides the necessary knowledge of density profiles to appropriately model the predicted soft X-ray emissions within the cusp.

2. Instrumentation

The Polar spacecraft was launched in February 1996 into an eccentric polar orbit ($9.5 R_E \times 1.8 R_E$) with an orbital period close to 17.5 h. As the mission progressed, the line of apsides dropped, allowing observational coverage of the cusp at a range of radial distances from the Earth over the course of the mission. Figure 1 shows the progression of the orbit over time. The current study used measurements from 1998 to 2005 to monitor the cusp at a variety of radial distances.

In situ measurements of the cusp and adjacent magnetospheric regions were obtained from the Hot Plasma Analyzer (HYDRA) [*Scudder et al., 1995*], Electric Field Instrument (EFI) [*Harvey et al., 1995*], Magnetic Field Experiment (MFE) [*Russell et al., 1995*], and Magnetospheric Ion Composition Spectrometer (MICS) sensor. The MICS sensor was part of the Charge and Mass Magnetospheric Ion Composition Experiment (CAMMICE) on Polar. A similar instrument to MICS flew on CRRES [*Wilken et al., 1992*]. Bulk flow measurements used in this study were from HYDRA, while the electron density was from EFI. The MICS sensor separated incident ions by energy per charge through an electrostatic analyzer then identified the mass per charge through post acceleration and time of flight. The total energy is measured by measurement of the particle on a solid state detector. The system was able to measure fluxes of a number of ion species. Two presented in the present study are high charge state oxygen ($O^{>+2}$) and He^{++} with energy per charge (E/q) from 1 to 300 keV.

Solar wind densities were obtained from the OMNI database [*King and Papitashvili, 2005*] which are provided time propagated to the nose of the bow shock. A 1 min time resolution data are used. Uncertainties in the propagation [e.g., *Collier et al., 1998*] may lead to some scatter in the results of this study. An evaluation of how different errors in propagation time may impact the results is presented in section 3.1.2.

3. Observations

A conservative identification of the cusp was made using the criteria described below. Spatially, the spacecraft position was required to be within 1.5 h of noon in magnetic local time and between 70° and 85° in invariant latitude. The electron spectra were required to peak at $100 \text{ eV} \pm 50\%$, indicating shocked solar wind plasma. The duration of the encounter was required to exceed 5 min. Lastly, the bulk flow was required to be less than 150 km/s, to eliminate periods when the spacecraft was in the magnetosheath. In reality the cusp position can be outside of the spatial bins set up for this study; however, previous statistical studies at low [*Newell and Meng, 1992*] and high altitude [*Palmroth et al., 2001; Merka et al., 2002; Niehof et al., 2010*] have found the cusp

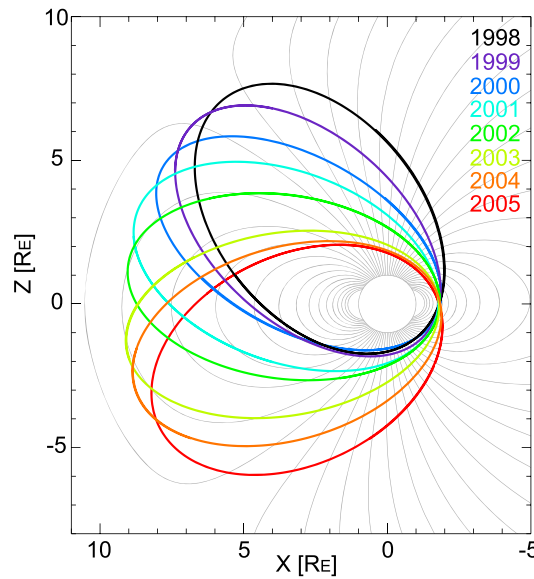


Figure 1. Orbit of the Polar spacecraft with time between 1998 and 2005 in GSE coordinates.

to be within this region the majority of the time, so our identification criteria identified sufficient cusp passes to monitor the changes in density with this criterion.

Two sample cusp crossings are shown in Figure 2, one at high altitude ($r \sim 8.5 R_E$) and one at lower altitude ($r \sim 2.3 R_E$). In the high-altitude pass on the left, the spacecraft passes from the dayside trapping region to the cusp to the lobe. Within the cusp there are increased fluxes of solar wind ions (He^{++} and $O^{>+2}$), indicative of solar wind plasma entry. The plasma transitions from a hot and tenuous plasma within the trapping region to a cool dense plasma with a peak in electron flux near 100 eV. The density and electron flux at 100 eV decreases as Polar passes into the lobe region.

The cusp magnetic field at high altitude is depressed and turbulent. This feature is often called a cusp diamagnetic cavity or “CDC” and is observed [e.g., Fritz et al., 2003; Walsh et al., 2007; Niehof et al., 2010] and modeled in the exterior cusp [Adamson et al., 2011]. Although the diamagnetic cavity can show clear boundaries that delineate the cusp at large radial distances, it is not as clear at smaller radial distances. The formation of the diamagnetic cavity is due to a pressure balance between the magnetic pressure of the geomagnetic field and the thermal pressure of the injected, shocked, solar wind plasma. If density stays constant along the magnetic field lines threading the cusp, and the magnitude of the magnetic field increases as $1/r^3$, the sharp gradients in the magnetic field at the edges of the cusp will disappear at lower radial distances. The absence of the diamagnetic cavity is seen in the low-altitude cusp pass in Figure 2 (right).

The cusp magnetic field at high altitude is depressed and turbulent. This feature is often called a cusp diamagnetic cavity or “CDC” and is observed [e.g., Fritz et al., 2003; Walsh et al., 2007;

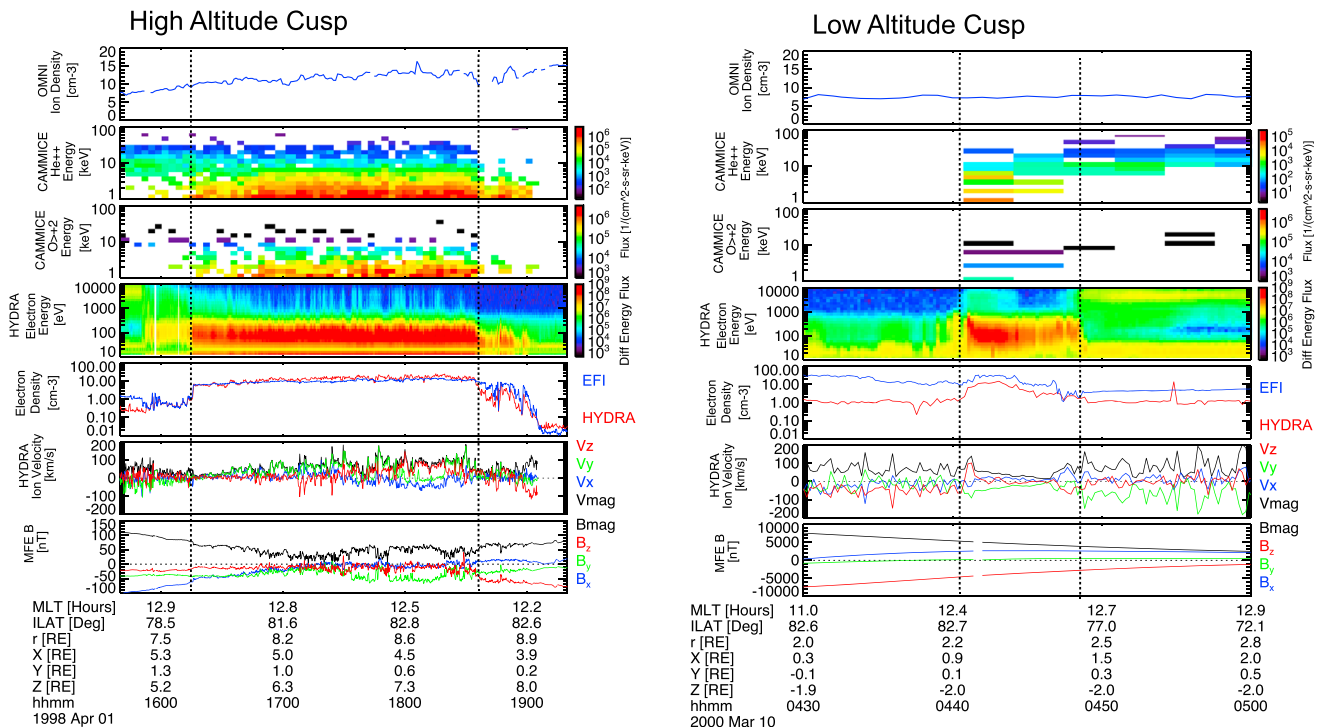


Figure 2. Sample cusp crossings from the Polar spacecraft at high and low altitudes. The top panel for each pass is density in the solar wind from the OMNI data set, while the rest are measured from the Polar spacecraft.

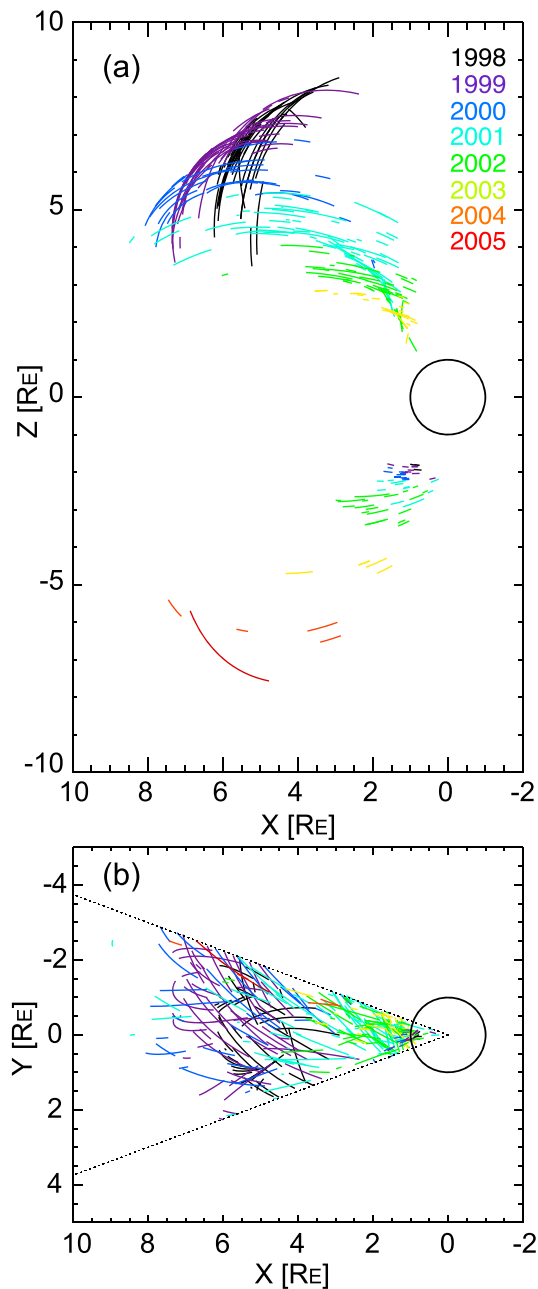


Figure 3. Positions of Polar during cusp crossings in GSM coordinates in the (a) XZ and (b) XY planes. The trajectories are colored by the year when the observations were made.

The variable depth of the cusp diamagnetic cavity is also observed with statistical maps from Polar [Zhou *et al.*, 2001], Cluster [Lavraud *et al.*, 2004], and statistical studies with combined spacecraft [Tsyganenko, 2009].

In the low altitude cusp, shown in Figure 2 (right), Polar passes from the lobe to the cusp to the dayside trapping region. Once again, observations of the cusp presents increased flux of solar wind plasma, identified from the 100 eV electrons. The cusp pass at low altitude has a duration of less than 10 min. The size of the cusp is typically smaller at low altitudes, while the velocity of Polar is greater. Some enhancements of He⁺⁺ and O^{>+2} can be seen, but fluxes were low. In this region, EFI densities from the spacecraft potential exceed those from HYDRA particle measurements. This implies the presence of a cold plasma population below the threshold of the HYDRA detector (~5 eV). One may also be concerned that this is a result of a calibration issue

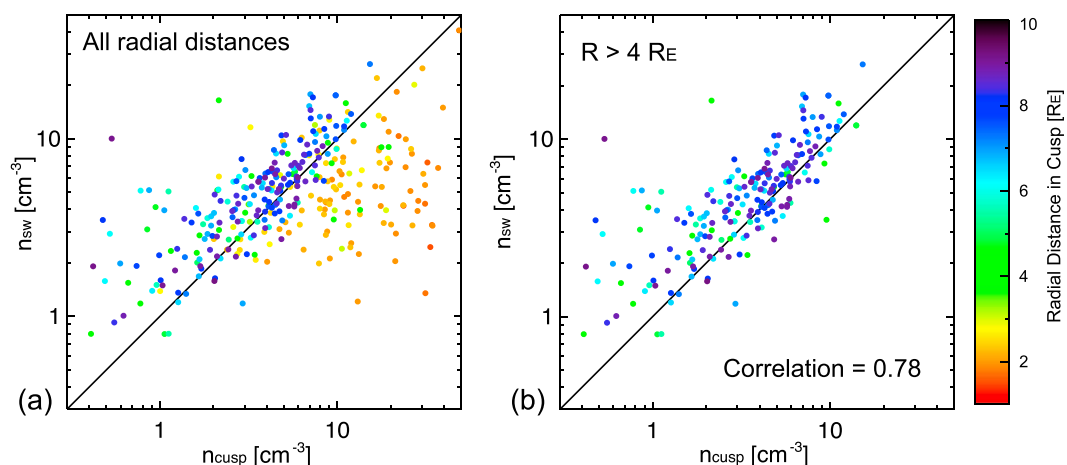


Figure 4. Density measurements within the cusp from EFI on Polar compared to solar wind density from OMNI. Each point represents the median density during one cusp crossing. The color represents the mean radial distance of the spacecraft during the cusp crossing. (a) All cusp crossings, while (b) crossings with radial distances greater than $4 R_E$.

between the two instruments. Since the discrepancy is present in both the north and south cusps and only at low altitudes, it is likely that this is real and due to the presence of cold plasma.

3.1. Statistical Results

Using the conservative cusp criteria defined above, 337 cusp passes from Polar were identified from 1998 through 2005. Figure 3 presents the spatial positions of each cusp pass colored by year of observation. The sampling covers a wide range of radial distances, and the shape of the converging field lines can clearly be seen. Due to the precession of the orbit, fewer samples were available in the southern cusp.

3.1.1. Density Profiles

Mid- and high-altitude cusp densities track solar wind densities closely. This is consistent with results from the Viking spacecraft [Aparicio et al., 1991]. Figure 4 presents the density in the cusp as a function of the solar wind density. Each point represents one spacecraft pass through the cusp. The median solar wind and cusp densities during the pass are plotted. When Polar is within the cusp at radial distances greater than $\sim 4 R_E$, the cusp densities track those within the solar wind closely, indicating efficient and rapid solar wind entry (Figure 4b). As solar wind densities change, cusp densities change quickly reflecting the change. Cusp and solar wind densities are well correlated (Pearson correlation coefficient of 0.78) over the order of magnitude variations in solar wind density observed during these cusp passes.

At radial distances less than $\sim 4 R_E$ the density in the cusp is often larger than that in the solar wind (Figure 4a). This is likely a result of multiple sources of plasma in the cusp. In the mid- and high-altitude cusp, the primarily population consists of shocked solar wind plasma. At low altitudes the cusp also has significant contributions from the ionosphere. A display of the cusp densities scaled by solar wind density is given with spatial positions in Figure 5. Each point represents the mean position of one cusp passage, and the cusp and solar wind density is the median values during the passage. The increase in cusp density at low altitude is seen in both the northern and southern hemispheres. The increase in cusp density to values greater than the solar wind density is likely due to contributions from the ionosphere (see the reviews André and Yau [1997] and Yau and André [1997]).

With these measurements, one can also quantify the density of solar wind plasma in the cusp. Figure 6 presents statistics of the density ratio ($n_{\text{cusp}}/n_{\text{sw}}$) as a function of radial distance. The cross bar in each blue box is the median, while the top and bottom of each box are the first and third quartiles of the data in each $0.5 R_E$ radial distance bin. The blue whiskers extend to 1.5 times the interquartile range. Similar to the treatment of the data above and in Figure 4, the discussion of the density ratio is separated to focus on radial distances first greater than and then less than $4 R_E$. The separation allows us to roughly isolate regions dominated by different sources, the solar wind and the ionosphere.

At radial distances in the cusp greater than $4 R_E$, the median density ratio ($n_{\text{cusp}}/n_{\text{sw}}$) ranges between 0.55 and 0.84. Although the median value shows some variability, there is no clear trend for the cusp density to increase or decrease with radial distance in the middle- and high-altitude cusps. A nearly steady solar wind density ratio

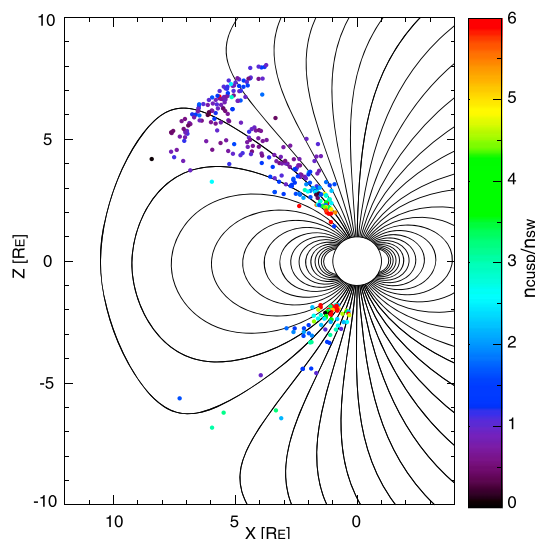


Figure 5. Spatial position of cusp crossings colored by the ratio of cusp density over the solar wind density. Each point represents one cusp passage. The spatial position of each point is the mean position during the cusp crossing. The density from Polar was obtained from EFI.

with decreasing radial distance in this range is consistent with predictions of the Liouville Theorem. Although some particles mirror and bounce out of the cusp where the magnitude of the magnetic field becomes larger, field lines also converge which bring more particles into a smaller area. When all points at $r > 4 R_E$ are included, the median cusp density is 80% of that in the solar wind. Statistical surveys have shown that in the magnetosheath density adjacent to the dayside magnetopause ranges from ~ 2 to 5 times that in the solar wind [Walsh et al., 2012; Dimmock and Nykyri, 2013]. Although the density in the middle- and high-altitude cusp scales with that in the solar wind, the magnitude is less than that in the adjacent magnetosheath.

At radial distances less than $4 R_E$, the median density ratio increases with decreasing radial distance from a value of 0.76 at $4.0\text{--}4.5 R_E$ to 2.98 at the lowest altitude bin surveyed ($2.0\text{--}2.5 R_E$). With decreasing radial distance the range of the density ratio also increases, shown in the first and third quartiles of the data. Since the drivers of ion outflow in the cusp can be highly time dependent, large variability in density from the ionosphere would be anticipated at low altitudes. This density profile as a function of radial distance is consistent with these predictions. Although solar wind plasma dominates in the middle- and high-altitude cusp, contributions from the ionosphere begin to become significant near $\sim 4 R_E$ where the density and variability increase with decreasing radial distance.

3.1.2. Speed of Entry

Solar wind plasma enters the cusp rapidly. To look for possible delays in the entry of solar wind plasma, the time period used to obtain solar wind density was shifted to up to a maximum value of ± 30 min by intervals of

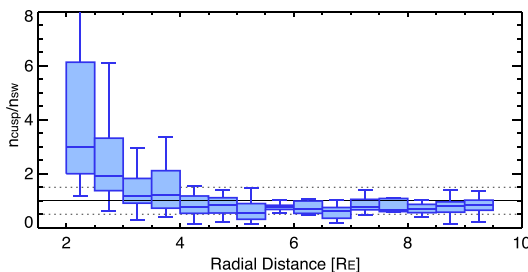


Figure 6. Ratio of cusp density over the solar wind density as a function of radial distance from the Earth. Polar density measurements are from EFI, while the solar wind density is from OMNI. The blue box presents the median, first, and third quartiles for data in each $0.5 R_E$ bin. The blue whiskers extend to 1.5 times the interquartile range.

1 min. The Pearson correlation coefficient between the cusp densities observed by Polar and the time-shifted solar wind density from OMNI was then calculated. The results are presented in Figure 7. To avoid cusp measurements where the density may be dominated by ionospheric contributions, passes with a mean radial distance less than $4 R_E$ were excluded, as done in Figure 4b. The correlation coefficient peaks at -3 min. A peak in correlation coefficient with a positive time delay would indicate it takes a finite time delay for the plasma to enter the cusp. A negative offset (as observed here) indicates that a density increase in the cusp occurs before one in the solar wind. Although a negative delay is shown here, it is a nonphysical

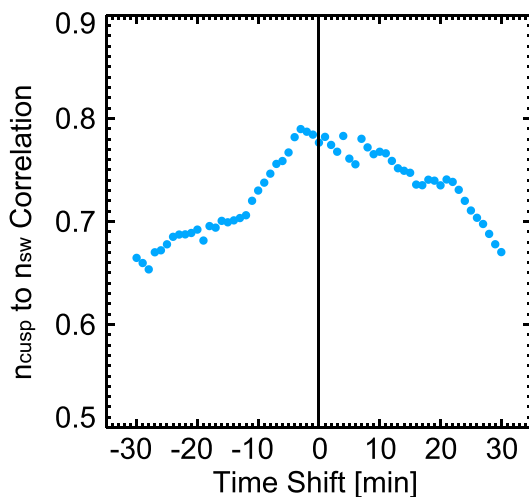


Figure 7. Correlation coefficient between density in the cusp from Polar and time-shifted solar wind density from OMNI (points shown in Figure 4b). The Pearson correlation coefficient peaks with a small delay indicating rapid entry of solar wind plasma into the cusp.

high charge state oxygen ($O^{>+2}$) in the cusp calculated with measurements from the MICS detector is presented as a function of solar wind density in Figure 8. Just as in Figure 4, each point in Figure 8 represents the median values during one cusp pass. Once again, there is a positive trend between the cusp and the solar wind densities indicating the efficient entry of high charge state and heavy ions. In the case of $O^{>+2}$ there is significantly more scatter than that seen in the scaling between solar wind and cusp electron density. The Pearson correlation coefficient between the two sets is 0.38. This discrepancy is likely due to the limitations of the detector for this measurement. The energy range of the MICS detector does not capture the core of the oxygen particle distribution, so the calculated densities are underestimates of the true values. Changes in the shape of the distribution mean the underestimate of the density is not systematic. Additionally, the $O^{>+2}$ density values include larger error due to lower counting statistics. (Further description of the calculation of

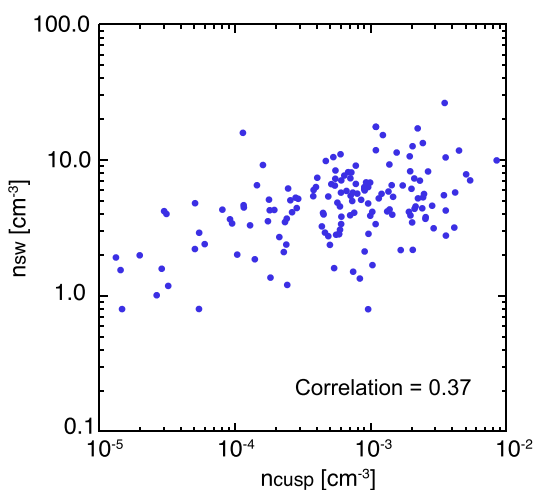


Figure 8. Density of high charge state oxygen ($O^{>+2}$) within the cusp as a function of solar wind density. The oxygen particle measurements are made by the MICS sensor on the CAMMICE instrument. Solar wind densities are from OMNI. Each point represents the median density value during a single cusp crossing. Cusp crossings at a radial distance greater than $4 R_E$ are plotted, similar to Figure 4b.

result and is likely a product of the error in propagation used. The OMNI data set time lags the solar wind data from spacecraft orbiting L1 to the nose of the bow shock. This process includes error due a number of effects including the position of the spacecraft relative to the Earth-Sun line as well as poor identification of the orientation of solar wind structural fronts. In an effort to study the entry speed of the solar wind, the fact that the delay to obtain the peak correlation coefficient is small, and even negative in this case, indicates that the solar wind has rapid entry.

3.2. High Charge State Solar Wind Ions

The ionization state of heavy ions such as oxygen can be used as tracers of their origin. High charge state ions observed within the magnetosphere are typically of solar wind origin, while lower charge states typically come from the ionosphere. The density of

the density from the MICS measurements is included in Appendix A.) These observational limitations prevent a quantitative analysis of how the density of high charge state ions may vary with radial distance or position within the cusp; however, a positive trend with solar wind density can be established.

4. Magnetohydrodynamics

The multifluid Block-Adaptive-Tree Solar Wind Roe-Type Upwind Scheme (BATSRUS) model [Powell et al., 1999; Tóth et al., 2005; Glocer et al., 2009; Tóth et al., 2012] was run to monitor the relative density contributions within the cusp in MHD. Two separate fluids were tracked in the model, one from the solar wind originating at the upstream boundary and one from the ionosphere originating at the inner boundary. By separating the ionospheric and solar wind fluids, the two populations can counterstream and produce more realistic cusp dynamics than a single-fluid approach

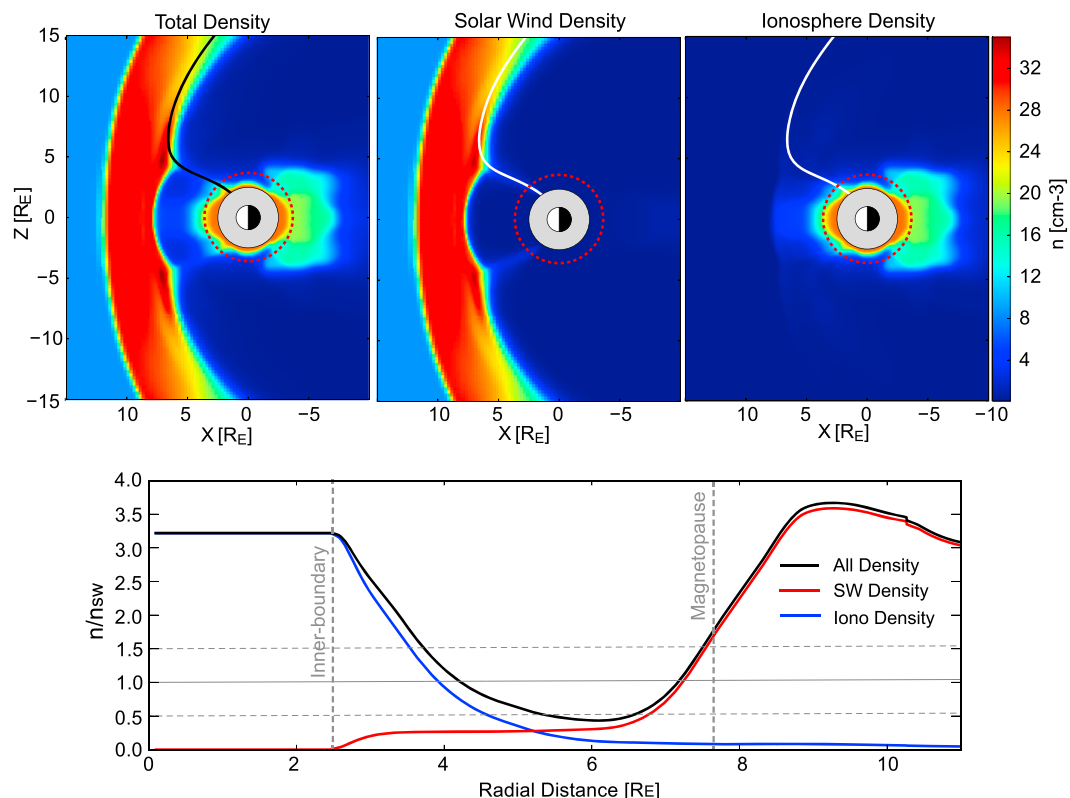


Figure 9. Multifluid BATSUS densities. (top) The total density, solar wind fluid density, and ionosphere fluid density from left to right in the GSM $Y = 0$ plane. The same magnetic field line is traced through the cusp for each plot. The red dashed circle is at a radial distance of $4 R_E$. (bottom) The densities along a field line as a function of radial distance in the cusp. The densities are normalized by the solar wind density, similar to the presentation in Figure 6.

[Welling and Liemohn, 2014]. The inner boundary is at $2.5 R_E$. The multifluid MHD run was initialized with 4 h of steady upstream conditions. The upstream parameters in GSM coordinates were held constant at $V[x, y, z] = [-450, 0, 0]$ km/s, $B[x, y, z] = [0, 0, -10]$ nT and $n_{sw} = 8.7 \text{ cm}^{-3}$. The density at the inner boundary was set to 28 cm^{-3} . The grid spacing in the low- and medium-latitude cusp ($r < 5 R_E$) is $1/16 R_E$ and $1/8 R_E$ at larger radial distances. Figure 9 (top) presents the densities in the GSM $Y = 0$ plane. A magnetic field line threading the cusp is traced and plotted in each density slice. Since the cusp topology follows magnetic field lines, the use of a field line provides a better map of the radial extent than a straight line. The field line is used to trace the cusp for Figure 9 (bottom).

The multifluid MHD model described above performs well in producing trends observed by Polar. Just as in the spacecraft measurements, the model shows that plasma of solar wind origin dominates the density in the exterior cusp, while by plasma of ionosphere origin dominates densities in the low altitude cusp. Figure 9 (bottom) presents the relative contributions to the total plasma density as a function of radial distance in a similar format to that of Figure 6. At low altitude, the model indicates that the total density in the cusp exceeds that in solar wind at a radial distance near $4.2 R_E$ and continues to increase with decreasing altitude due to increasing contributions from the ionosphere. Polar observes this transition to occur at radial distances from 3.5 to $4.0 R_E$. Although the model reproduces the density trend observed by Polar, the radial position of this transition does not match precisely, and there are several reasons why this behavior is expected. First, while ionospheric outflow is driven by many processes, both kinetic and fluid [see, e.g., Welling et al., 2015, and references therein], only a handful of outflow processes are captured in MHD without including a stand-alone outflow model [Welling and Liemohn, 2014]. This is especially true in the cusp.

By contrast to the trend successfully reproduced at low altitude, the multifluid MHD does not appropriately describe the behavior of the density in the exterior cusp. The model predicts the density of solar wind plasma in the cusp to increase with radial distance continuously up to the magnetopause. The large contribution of solar wind plasma even causes the total density in the cusp to increase to levels greater than the solar wind

near the magnetopause. This trend is not observed within the Polar measurements. Polar observes the density in the cusp to remain approximately constant (Figure 6) with increasing radial distance beyond $r \sim 4R_E$.

In addition to the ion outflow described above, there are additional reasons why there may be discrepancies. The cusp is often defined through kinetic features such as precipitating solar wind particles and energy dispersions. These features are not included in MHD, and their absence may contribute to the estimate of solar wind plasma in the cusp by MHD. Another feature which could impact the treatment of the cusp is the grid cell resolution. Previous MHD simulations have shown the spatial extent of the cusp to be a function of the resolution [Zhang *et al.*, 2013]; therefore, the plasma entry and density are also likely to depend on the resolution.

5. Conclusion

Statistical observations from the Polar spacecraft show the density in the mid- and high-altitude cusp ($r > 4R_E$) to be fairly constant at $\sim 80\%$ of that in the solar wind. The scaling with real-time solar wind density confirms rapid entry of solar wind plasma into the cusps. At radial distances less than $4R_E$ the cusp density increases to values greater than that within the solar wind, indicating contributions from the ionosphere which can dominate the total density in the cusp. The range of density ratio ($n_{\text{cusp}}/n_{\text{sw}}$) values also increases in the low-altitude cusp, indicating variable rates of ion outflow from the ionosphere. The density of high charge state oxygen (O^{7+}) displays a positive trend with solar wind density within the cusp. Multifluid MHD modeling was conducted to show the relative contributions of an ionospheric plasma and a solar wind plasma. The results were consistent with the Polar observations and confirmed the ionospheric contributions at low altitude.

Appendix A: MICS Density Calculations

High charge state oxygen densities were calculated by integrating the distribution function derived from the MICS differential number flux j , in $1/(\text{s cm}^2 \text{ sr keV/e})$. (The MICS fluxes are expressed as a function of energy per charge, resulting from selection by the electrostatic analyzer.) The distribution function f in terms of the flux, in energy space, is [e.g., Lyons and Williams, 1984, equation 2.67]

$$f = \frac{j m^2}{2E} \quad (\text{A1})$$

The three-dimensional velocity differential in pitch angle α and gyrophase ϕ

$$d\mathbf{v} = v^2 dv \sin \alpha d\alpha d\phi = \frac{\sqrt{2E}}{m^{3/2}} dE \sin \alpha d\alpha d\phi \quad (\text{A2})$$

The number density is the zeroth velocity moment (i.e., the integral over all velocities):

$$n = \int f d\mathbf{v} = \int_{\phi} \int_{\alpha} \int_E \frac{j m^2 \sqrt{2E}}{2E m^{3/2}} dE \sin \alpha d\alpha d\phi \quad (\text{A3})$$

or assuming gyrotropy and expressing in terms of energy per charge (the measurement MICS makes):

$$n = \sqrt{\frac{2m}{q}} \pi \int_{\alpha} \int_{\frac{E}{q}} \frac{j}{\sqrt{\frac{E}{q}}} \frac{dE}{q} \sin \alpha d\alpha \quad (\text{A4})$$

This integral was calculated numerically, using Simpson's method, first over energy and then over pitch angle, for each complete energy sweep of MICS (approximately 3 min or 16 spins of Polar.) No attempt was made to extrapolate beyond MICS coverage in either energy or pitch angle. The larger the angle (0° to 90°) between the field vector and the spin plane, the larger the MICS pitch angle coverage; this was the case for many high-altitude cusp passes, with the associated depressed and variable magnetic field.

The minimum MICS E/q of 1 keV/e was usually above the spectral peak in the cusp. Figure A1 shows the high charge state (normally 6+) oxygen flux from three cusp passes, including the two in Figure 2. It is clear that on the 1998 April and 2000 March passes, the peak in the plasma flux was below the MICS energy range; for 1999 April, it may have been just at the bottom of the range. Also clear are the fairly low counting statistics,

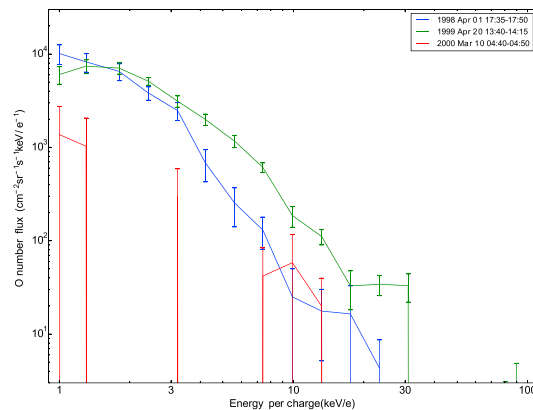


Figure A1. High charge state (commonly 6+) oxygen spectra for several cusp crossings. Error bars represent uncertainty from counting statistics and on board data compression. The three traces represent the spectra from cusp passes on 1 April 1998 (blue), 20 April 1999 (green), and 10 March 2000 (red). The 1998 and 2000 cusp crossings are also included in Figure 2.

particularly on the shorter low-altitude cusp passes. Comparison with total ion densities from moments of the HYDRA measurements indicates that the MICS densities were lower by a factor of order 40, although this reduction depends on the shape of the distribution.

Further simplifications include an assumption that the spacecraft potential was not of sufficient magnitude to modify the distribution, reasonable even at the minimum MICS energy of 1 keV/e. MICS only samples across one angle, as the spacecraft spins; the resulting changes in measured flux were assumed to be due entirely to changes in the pitch angle measured, which requires an assumption both of gyrotropy and that the field is stationary in the spacecraft frame. Motion was assumed nonrelativistic; a 200 keV/e O^{+6} ion would have a Lorentz factor $\gamma = 1.00008$.

Acknowledgments

Support was given by the NASA grant NNX14AK41G. The authors acknowledge the use of the SPEDAS analysis software. Analysis of the MHD results was performed using the Spacepy software library [Morley *et al.*, 2011]. Data used in this study are openly accessible from NASA's Coordinate Data Analysis Web (CDAWEB). The CAMMICE/MICS data can be obtained from <http://spacedata.bu.edu/mics.html>.

References

- Adamson, E., A. Otto, and K. Nykyri (2011), 3-D mesoscale MHD simulations of a cusp-like magnetic configuration: Method and first results, *Ann. Geophys.*, *29*, 759–770.
- André, M., and A. Yau (1997), Theories and observations of ion energization and outflow in the high latitude magnetosphere, *Space Sci. Rev.*, *80*, 27–48.
- Aparicio, B., B. Thelin, and R. Lundin (1991), The polar cusp from a particle point of view: A statistical study based on Viking data, *J. Geophys. Res.*, *96*, 14,023–14,031.
- Carter, J. A., S. Sembay, and A. M. Read (2011), Identifying XMM-Newton observations affected by solar wind charge exchange: Part II, *Astron. Astrophys.*, *527*, A115, doi:10.1051/0004-6361/201015817.
- Collier, M. R., J. A. Slavin, R. P. Lepping, A. Szabo, and K. Ogilvie (1998), Timing accuracy for the simple planar propagation of magnetic field structures in the solar wind, *Geophys. Res. Lett.*, *25*, 2509–2512, doi:10.1029/98GL00735.
- Collier, M. R., et al. (2014), On lunar exospheric column densities and solar wind access beyond the terminator from ROSAT soft X-ray observations of solar wind charge exchange, *J. Geophys. Res. Planets*, *119*, 1459–1478, doi:10.1002/2014JE004628.
- Cravens, T. E. (1997), Comet Hyakutake X-ray source: Charge transfer of solar wind heavy ions, *Geophys. Res. Lett.*, *24*, 105–108.
- Cravens, T. E., I. P. Robertson, and S. L. Snowden (2001), Temporal variations of geocoronal and heliospheric X-ray emission associated with the solar wind interaction with neutrals, *J. Geophys. Res.*, *106*(A11), 24,883–24,892, doi:10.1029/2000JA000461.
- Dennerl, K. (2002), Discovery of X-rays from Mars with Chandra, *Astron. Astrophys.*, *394*, 1119–1128, doi:10.1051/0004-6361:20021116.
- Dennerl, K., V. Burwitz, J. Englhauser, C. Lisse, and S. Wolk (2002), Discovery of X-rays from Venus with Chandra, *Astron. Astrophys.*, *386*, 319–330, doi:10.1051/0004-6361:20020097.
- Dimmock, A. P., and K. Nykyri (2013), The statistical mapping of magnetosheath plasma properties based on THEMIS measurements in the magnetosheath interplanetary medium reference frame, *J. Geophys. Res. Space Physics*, *118*, 4963–4976, doi:10.1002/jgra.50465.
- Escoubet, C. P., M. F. Smith, S. F. Fung, P. C. Anderson, R. A. Hoffman, E. M. Baasinska, and J. M. Bosqued (1992), Staircase ion signature in the polar cusp: A case study, *Geophys. Res. Lett.*, *19*, 1735–1738, doi:10.1029/92GL01806.
- Escoubet, C. P., et al. (2008), Effect of a northward turning of the interplanetary magnetic field on cusp precipitation as observed by Cluster, *J. Geophys. Res.*, *113*, A07513, doi:10.1029/2007JA012771.
- Farrell, W. M., and J. A. Van Allen (1990), Observations of the Earth's polar cleft at large radial distances with the Hawkeye 1 magnetometer, *J. Geophys. Res.*, *95*, 20,945–20,958.
- Frank, L. A. (1971), Plasma in the Earth's polar magnetosphere, *J. Geophys. Res.*, *76*(22), 5202–5219.
- Fritz, T. A., J. Chen, and G. L. Siscoe (2003), Energetic ions, large diamagnetic cavities, and Chapman-Ferraro cusp, *J. Geophys. Res.*, *108*(A1), 1028, doi:10.1029/2002JA009476.
- Fujimoto, M., K. Mitsuda, D. McCamman, Y. Takei, M. Bauer, Y. Ishisaki, F. S. Porter, H. Yamaguchi, K. Hayashida, and N. Yamasaki (2007), Evidence for solar-wind charge-exchange X-ray emission from the Earth's magnetosheath, *Publ. Astron. Soc. Jpn.*, *59*, S133–S140.

- Glocer, A., G. Tóth, Y. Ma, T. Gombosi, J.-C. Zhang, and L. M. Kistler (2009), Multifluid Block-Adaptive-Tree Solar Wind Roe-Type Upwind Scheme: Magnetospheric composition and dynamics during geomagnetic storms—Initial results, *J. Geophys. Res.*, *114*(A12), A12203, doi:10.1029/2009JA014418.
- Haerendel, G., G. Paschmann, N. Scokopke, H. Rosenbauer, and P. C. Hedgecock (1978), The frontside boundary layer of the magnetosphere and the problem of reconnection, *J. Geophys. Res.*, *83*(A7), 3195–3216, doi:10.1029/JA083iA07p03195.
- Harvey, P., et al. (1995), The GGS/Polar magnetic fields investigation, in *The Global Geospace Mission*, edited by C. Russell, pp. 583–596, Kluwer Acad., Norwell, Mass.
- Heikkila, W. J., and J. D. Winningham (1971), Penetration of magnetosheath plasma to low altitudes through the dayside magnetospheric cusps, *J. Geophys. Res.*, *76*, 883–891, doi:10.1029/JA076i004p00883.
- King, J. H., and N. E. Papitashvili (2005), Solar wind spatial scales in and comparisons of hourly Wind and ACE plasma and magnetic field data, *J. Geophys. Res.*, *110*, A02104, doi:10.1029/2004JA010649.
- Kremser, G., J. Woch, K. Mursula, P. Tanskanen, B. Wilken, and R. Lundin (1995), Origin of energetic ions in the polar cusp inferred from ion composition measurements by the Viking satellite, *Ann. Geophys.*, *13*, 595–607, doi:10.1007/s00585-995-0595-9.
- Kuntz, K. D., et al. (2015), The solar wind charge-exchange production factor for hydrogen, *Astrophys. J.*, *808*, 143, doi:10.1088/0004-637X/808/2/143.
- Lavraud, B., A. Fedorov, E. Budnik, A. Grigoriev, P. J. Cargill, M. W. Dunlop, H. Rème, I. Dandouras, and A. Balogh (2004), Cluster survey of the high-altitude cusp properties: A three-year statistical study, *Ann. Geophys.*, *22*, 3009–3019.
- Lockwood, M. (1995), Overlapping cusp ion injections: An explanation invoking magnetopause reconnection, *Geophys. Res. Lett.*, *22*, 1141–1144.
- Lockwood, M., and M. F. Smith (1994), Low and middle altitude cusp particle signatures for general magnetopause reconnection rate variations: 1. Theory, *J. Geophys. Res.*, *99*, 8531–8553, doi:10.1029/JA093iA12p14549.
- Lyons, L. R., and D. J. Williams (1984), *Quantitative Aspects of Magnetospheric Physics*, D. Reidel, Dordrecht, Netherlands.
- Merka, J., J. Šafránková, and Z. Němeček (2002), Cusp-like plasma in high altitudes: A statistical study of the width and location of the cusp from Magion-4, *Ann. Geophys.*, *20*, 311–320.
- Morley, S., D. Welling, J. Koller, B. A. Larsen, M. G. Henderson, and J. Niehof (2011), SpacePy—A Python-based library of tools for the space sciences, in *Proceeding of the 9th Python in Science Conference*, edited by S. van der Walt and J. Millman, pp. 39–45, Austin, Tex.
- Newell, P. T., and C.-I. Meng (1991), Ion acceleration at the equatorward edge of the cusp: Low-altitude observations of patchy merging, *Geophys. Res. Lett.*, *18*, 1829–1832.
- Newell, P. T., and C. T. Meng (1992), Mapping the dayside ionosphere to the magnetosphere according to particle precipitation characteristics, *Geophys. Res. Lett.*, *19*, 609–612, doi:10.1029/92GL00404.
- Newell, P. T., and C. T. Meng (1988), The cusp and the cleft/LLBL: Low-altitude identification and statistical local time variation, *J. Geophys. Res.*, *93*, 14,549–14,556, doi:10.1029/JA093iA12p14549.
- Niehof, J. T., T. A. Fritz, R. H. W. Friedel, and J. Chen (2010), Size and location of cusp diamagnetic cavities observed by Polar, *J. Geophys. Res.*, *115*, A07201, doi:10.1029/2009JA014827.
- Palmroth, M., H. Laakso, and T. I. Pulkkinen (2001), Location of high-altitude cusp during steady solar wind conditions, *J. Geophys. Res.*, *106*, 21,109–21,122, doi:10.1029/2001JA900073.
- Perry, C. H., M. Grande, T. H. Zurbuchen, S. Hefti, G. Gloeckler, J. F. Fennell, B. Wilken, and T. A. Fritz (2000), Use of Fe charge state changes as a tracer for solar wind entry to the magnetosphere, *Geophys. Res. Lett.*, *13*, 2441–2444, doi:10.1029/2000GL003780.
- Pitout, F., C. P. Escoubert, B. Klecker, and I. Dandouras (2009), Cluster survey of the mid-altitude cusp—Part 2: Large-scale morphology, *Ann. Geophys.*, *27*, 1873–1886, doi:10.5194/angeo-27-1875-2009.
- Powell, K. G., P. L. Roe, T. J. Linde, T. I. Gombosi, and D. L. De Zeeuw (1999), A solution-adaptive upwind scheme for ideal magnetohydrodynamics, *J. Comput. Phys.*, *154*, 284–309.
- Reiff, P. H., T. W. Hill, and J. L. Burch (1977), Solar wind plasma injection at the dayside magnetospheric cusp, *J. Geophys. Res.*, *82*(4), 479–491.
- Robertson, I. P., M. R. Collier, T. E. Cravens, and M.-C. Fok (2006), X-ray emission from the terrestrial magnetosheath including the cusps, *J. Geophys. Res.*, *111*, A12105, doi:10.1029/2006JA011672.
- Rosenbauer, H., H. Grunwaldt, M. D. Montgomery, G. Paschman, and N. Scokopke (1975), Heos 2 plasma observations in the distant polar magnetosphere: The plasma mantle, *J. Geophys. Res.*, *80*, 2723–2737.
- Russell, C. T., R. C. Snare, J. D. Means, D. Pierce, D. Dearborn, M. Larson, G. Barr, and G. Le (1995), The GGS/Polar magnetic fields investigation, *Space Sci. Rev.*, *71*, 563–582, doi:10.1007/BF00751341.
- Scudder, J. D., et al. (1995), Hydra—A 3-dimensional electron and ion hot plasma instrument for the Polar spacecraft of the GGS mission, in *The Global Geospace Mission*, edited by C. Russell, pp. 459–495, Kluwer Acad., Norwell, Mass.
- Shelley, E. G., R. D. Sharp, and R. G. Johnson (1976), He⁺⁺ and H⁺ flux measurements in the dayside cusp: Estimates of convection electric field, *J. Geophys. Res.*, *81*, 2363–2360.
- Smith, M. F., and M. Lockwood (1990), The pulsating cusp, *Geophys. Res. Lett.*, *17*, 1069, doi:10.1029/GL017i008p01069.
- Snowden, S. L., M. R. Collier, and K. D. Kuntz (2004), XMM-Newton observation of solar wind charge exchange emission, *Astrophys. J.*, *610*, 1182–1190.
- Tóth, G., et al. (2005), Space Weather Modeling Framework: A new tool for the space science community, *J. Geophys. Res.*, *110*, A12226, doi:10.1029/2005JA011126.
- Tóth, G., et al. (2012), Adaptive Numerical Algorithms in Space Weather Modeling, *J. Comput. Phys.*, *231*, 870–903.
- Trattner, K. J., A. J. Coates, A. N. Fazakerley, A. D. Johnstone, H. Balsiger, J. L. Burch, S. A. Fuselier, W. K. Peterson, H. Rosenbauer, and E. G. Shelley (1998), Overlapping ion populations in the cusp: Polar/TIMAS results, *Geophys. Res. Lett.*, *20*, 1621–1624, doi:10.1029/98GL01060.
- Tsyganenko, N. A. (2009), Magnetic field and electric currents in the vicinity of polar cusps as inferred from Polar and Cluster data, *Ann. Geophys.*, *27*, 1573–1582.
- Walsh, B. M., T. A. Fritz, N. M. Lender, J. Chen, and K. E. Whitaker (2007), Energetic particles observed by ISEE-1 and ISEE-2 in a cusp diamagnetic cavity on 29 September 1978, *Ann. Geophys.*, *25*, 1–8.
- Walsh, B. M., D. G. Sibeck, Y. Wang, and D. H. Fairfield (2012), Dawn-dusk asymmetries in the Earth's magnetosheath, *J. Geophys. Res.*, *117*, A12211, doi:10.1029/2012JA018240.
- Wargelin, B. J., M. Markevitch, M. Juda, V. Kharchenko, R. Edgar, and A. Dalgarno (2004), Chandra observations of the “dark” Moon and geocoronal solar wind charge exchange, *Astrophys. J.*, *607*, 596–610, doi:10.1086/383410.
- Welling, D. T., and M. W. Liemohn (2014), Outflow in global magnetohydrodynamics as a function of a passive inner boundary source, *J. Geophys. Res. Space Physics*, *119*, 2691–2705, doi:10.1002/2013JA019374.

- Welling, D. T., et al. (2015), The Earth: Plasma sources, losses, and transport processes, *Space Sci. Rev.*, 192(1–4), 145–208, doi:10.1007/s11214-015-0187-2.
- Wilken, B., W. Weiss, D. Hall, M. Grande, F. Soraas, and J. F. Fennell (1992), Magnetospheric ion composition spectrometer onboard the CRRES spacecraft, *J. Spacecr. Rockets*, 29(4), 585–591, doi:10.2514/3.25503.
- Woch, J., and R. Lundin (1992), Magnetosheath plasma precipitation in the polar cusp and its control by the interplanetary magnetic field, *J. Geophys. Res.*, 97(A2), 1421–1430, doi:10.1029/91JA02487.
- Yau, A. W., and M. André (1997), Sources of ion outflow in the high latitude ionosphere, *Space Sci. Rev.*, 80, 1–25.
- Zhang, B., O. Brambles, W. Lotko, W. Dunlap-Shohl, R. Smith, M. Wiltberger, and J. Lyon (2013), Predicting the location of polar cusp in the Lyon-Fedder-Mobarry global magnetosphere simulation, *J. Geophys. Res. Space Physics*, 118, 6327–6337, doi:10.1002/jgra.50565.1.
- Zhou, X. W., C. T. Russell, G. Le, S. A. Fuselier, and J. D. Scudder (2001), Factors controlling the diamagnetic pressure in the polar cusp, *Geophys. Res. Lett.*, 28, 915–918.